COMPREHENSIVE MODEL FOR ROTARY WING UNMANNED AERIAL VEHICLE

Fahri Ersel Olcer, ASELSAN Inc., MGEO Sec., Ankara, Turkey

Abstract

Comprehensive model of a rotary wing unmanned aerial vehicle is built and analyzed in this study. It is a conventional rotorcraft, except its size. It makes use of a fly-bar system providing some level of stabilization in the pitch and roll motions as well as alleviating control loads, therefore special attention is given on the modeling of this system. Its model is built using FLIGHTLAB commercial software by adopting its full rotorcraft template and customization by increasing the number of rotors to accommodate for fly-bar system, tuning the maneuver wake distortion model and generating custom controls associated with the fly-bar/main rotor interactions. Analyses are carried out to highlight nonlinear effects associated with the fly-bar mechanism which is a typical component used on the small size unmanned rotary vehicles.

NOTATION

A1S	Lateral Cyclic
B1S	Longitudinal Cyclic
MR	Main rotor
TR	Tail rotor
TPP	Tip Path Plane
τ_{RW}	Time constant of rotor wake
ν_i	Inflow ratio
θ	Pitch attitude
Φ	Roll attitude
μ	Advance ratio
K_p^{fb}	Equivalent rollrate feedback gain for fly-bar
K_q^{fb}	Equivalent pitchrate feedback gain for fly-bar
k_{pq}	Maneuver Wake Distortion rate scale factor

1. INTRODUCTION

Comprehensive model of a small size rotary wing unmanned aerial vehicle is built and analyzed in this study. It consists of a conventional main rotor-tail rotor configuration with the added fly-bar rotor system on top of the main rotor which provides some level of stabilization in the pitch and roll motions as well as alleviating control loads, therefore special attention is given on the modeling of this system. Its model is built using FLIGHTLAB commercial software [1] by adopting its full rotorcraft template and customizing it by increasing the number of rotors to accommodate for the fly-bar rotor system, tuning the maneuver wake distortion model and generating custom controls associated with the fly-bar/main rotor interactions. In order to justify the adopted modeling options and parameters, sensitivity analyses are carried out. Further analyses are also performed to highlight nonlinear effects associated with the fly-bar mechanism which is a typical component used on the small size unmanned rotary vehicles and limitations due to fly-bar are noted.

Modeling of the fly-bar system as a rotor, elastic main rotor blades and inflow dynamics due to main rotor and its effect over the fly-bar are significant improvements presented in the current work.

2. MODELING OF THE ROTARY WING UAV

2.1. Baseline Helicopter

The reference helicopter used in this study is a 38 kg, conventional rotorcraft. Its main rotor has two blades which are rigidly attached in flapping direction and each one had a hinge for lead-lag degree of freedom. Its diameter is 2.24 meter and it also incorporates two bladed fly-bar tilting rotor system about the size quarter of the main rotor diameter to provide stabilization and control load alleviation.

Modeling of the helicopter is accomplished using FLIGHTLAB by adopting its full rotorcraft model template. In this study special treatment is needed for modeling the fly-bar and wake dynamics which are explained in details in the following sections. Fuselage is modeled as a rigid body using mass and inertia properties, along with its aerodynamics where empirical formulas, found in [2], are translated into table look-ups with appropriate scaling values.

Blade Element Method is used for the modeling of all of the three rotors; main rotor, fly-bar, and tail rotor. One dimensional grid for each blade is constructed

with a particular sizing that fly-bar blade sections match inner sections of the main rotor blade at the same radial positions in order to provide a consistency in the modeling. Likewise, a higher order inflow model is used for the main rotor whereas uniform inflow assumption is adopted for the fly-bar and the tail rotor. Inflow field produced by the main rotor is an important contributor for the fly-bar inflow; therefore it is modeled using the rotor interference option. Though there are studies in the literature focusing on the coupled solution to the rotor-rotor interactions using generalized dynamic inflow models such as [3], main rotor to fly-bar interaction is fairly a one-way interaction considering the size difference between the rotors and the placement of the smaller fly-bar rotor which is located at the core of the main rotor; therefore such advanced methods are not necessary for the current study.

Engine dynamics, consequently the rotor speed degree of freedom is omitted in this study. Though it can alter the dynamics in case of significant rotor speed variation as it was observed in an earlier work [4], a reliable governor design makes it obsolete to include. Analyses in the current study are limited with the constant rotor speed assumption.

2.2. Fly-Bar Rotor System

Fly-bar is modeled as a standalone rotor by increasing the available number of rotors to three in the full rotorcraft model template available in FLIGHTLAB. Main rotor and fly-bar had become the rotors number one and two, and then third one is added for the tail rotor. Stabilization and control load alleviation of the fly-bar system arise due to the mechanical connections where tilting of the fly-bar teetering rotor contributes to the main rotor pitch. These connections are modeled as part of the control system which is carried out in the Control System Graphical Editor (CSGE) of the program. These connections consist of ball-end-links, same with those control connections between the swashplate and the direct blade controls on the original system. In the modeling phase all of these connections assumed to be rigid. More detailed properties of the fly-bar control system for a similar size helicopter can be found in the literature [5].

Objective of this approach is to account for the nonlinearities associated with the mechanical limits and more importantly rotor aeromechanics such as change in the flapping/teetering response of the fly-bar may not be necessarily linear as cyclic input increased, and there would be possible stall conditions. This capability is one of the distinguishing points of this work compared to earlier RW-UAV studies considering fly-bar as simple as a constant gain feedback system or making use of small angle assumptions [5].

2.3. Main Rotor Blades

Main rotor blades are attached to the hub through lead-lag hinges and bearings for feathering. There is no hinge associated with the flap degree of freedom but elasticity of the blades in this direction plays a significant role, especially for the tilt of the tip-path-plane and the phase lag between the inputs and the tilt of the TPP. Therefore this effect is addressed by a limited modal representation considering only the first flapping mode which is extracted by testing of a sample blade in a local mechanical testing facility. I order to perform this test, a sample blade is rotated 90 degrees in the feathering axis and then fixed to a rigid support at its root. 10 accelerometers are attached on the blade and wired to the data acquisition system. Single excitation of the blade in the flapping direction (parallel to the ground during testing in order to eliminate gravitational effects) provided sufficient data to estimate the modal stiffness and mode shape of the first flapping mode. Acquired information is used in the modal based elastic blade modeling of the program. Furthermore, stiffening effect due to rotational speed is estimated in the program, and the obtained fanplot considering only the first two modes is shown in Figure 1. Lead-lag degree of freedom is modeled by a hinge therefore its rotating natural frequency is dominated solely by the rotation speed at all times. Flap is also dominated by the rotational speed when it is over 25% of the nominal speed which increases the importance of the mode shape compared to its modal stiffness, both obtained at static conditions.

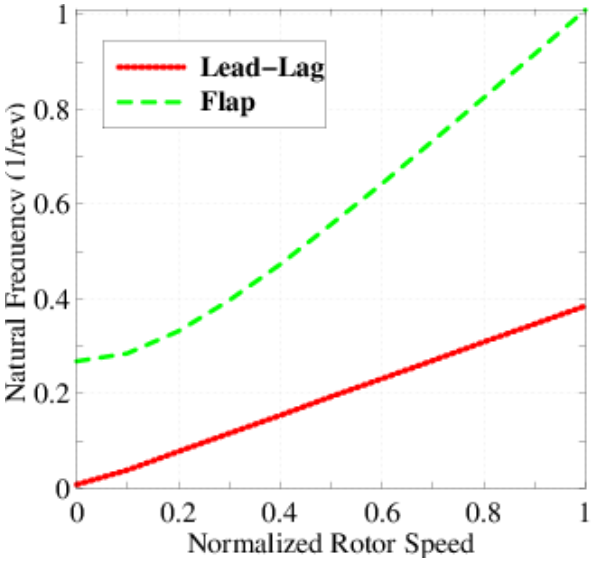

Figure 1 Main rotor natural frequencies

2.4. Control System

Control system of the current RW-UAV is embedded in homebuilt autopilot hardware. It is composed of feedback loops commanded by the target body velocities and heading. A development version of the controller is selected for the current study which produced distinguishing results during flight testing as shown in Figure 2. Therefore same feedback parameters are used in the modeling phase and similar responses are sought for model validation purposes. Its modeling is accomplished by translating the control blocks into the FLIGHTLAB's Control System Graphical Editor (CSGE), using elements like integrator, gain etc. Mechanical relations of the links within and between the main rotor and fly-bar systems are generated in this phase as well.

Navigation algorithms, which are also running on the same autopilot hardware, consist of pre-filtering of the measured data and usage of a high order Kalman filter. Numerical implementation of the pre-filter is identified as a transfer function using CIFER and it is embedded in the control model for the states used in the controller algorithms to account for the delay and smoothing of the filter. Besides autopilot response frequency is also implemented in the control system modeling by freezing the control system outputs for several time steps since the model runs at a much higher frequency even the number of azimuth steps is chosen as low as 72.

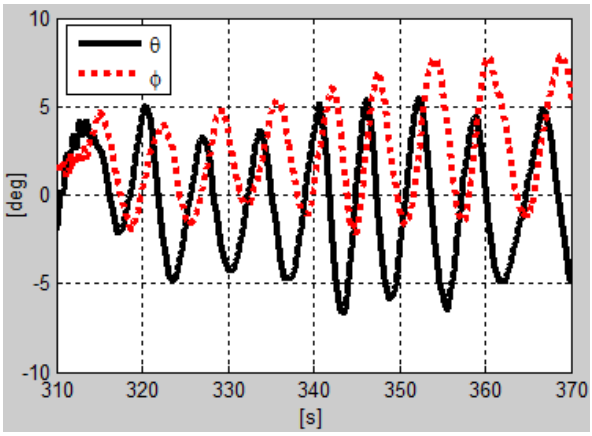

Figure 2 Pitch and roll oscillations during hovering flight test

Alternative approaches to the control system modeling is running the autopilot codes on a component level in FLIGHTLAB or on a separate dedicated autopilot card and maintaining a connection between one of those two alternatives and simulation software. These options constitute the software in the loop and hardware in the loop solutions but they should be considered for higher fidelity studies which might aim for high frequency or hardware issues related with the autopilot. Another approach which is a midway solution is to translate and run the codes under SIMULINK environment which can be run simultaneously with FLIGHTLAB on a step-by-step data sharing mode. This method is already verified and is currently in progress for the further studies. An outstanding advantage with the last tentative approach and the current one is to provide a physically more meaningful environment for the control designer to work with instead of stepping into the programming phase every time a change is considered.

2.5. Maneuver Wake Distortion Effect and Dynamic Inflow

Maneuver Wake Distortion (MWD) is an option available in FLIGHTLAB under Peters-He inflow model options to account for the dynamics of the wake geometry. Though Peters-He inflow model itself is actually a "dynamic" model, it does not account for the dynamics of the wake geometry (change in the orientation of the wake tube) when the body goes through pitch and roll motions. This phenomena was studied in the literature [6], and it was shown that including this effect significantly improves the transient responses, especially off-axis ones. A first order transfer function is used to emulate this issue in which its time constant is estimated using the empiric formula (1) from the literature.

$$\tau_{RW} = \frac{16}{15\pi \cdot v_i} \quad (1)$$

Wake distortion effect tables are also tuned to obtain physically meaningful results since default values available are associated with a full size rotorcraft. They are scaled down till reasonable responses are observed. It is also noted at this point that empirical formulas describing the relation between the body rotational rates and the rotor wake account for physical values such as rotor thrust, rotor speed and inflow velocity but the flapping stiffness (or flapping natural frequency) is not included among those parameters. Change in the flapping stiffness affects the time delay of the rotor disk motion with respect to body which in return effectively adds up to the delay between the body rates and the rotor wake. The need for adjustment of the parameters found through the empirical formulas might be justified due to this issue.

Moreover with the inflow modeling options, Three-State Peters-He inflow model is used and it is

updated by augmenting the inflow gain matrix (L-Matrix) with the predefined values. Both MWD and inflow model update are brought to their final values by analysis and comparison with the test data.

2.5.1. Analysis on the Maneuver Wake Distortion Parameters

Maneuver Wake Distortion parameters are concern of this study as they are found to be crucial for capturing the high amplitude oscillations observed during hovering tests when the controller is enabled. In order to capture the characteristics of the vehicle with an advanced nonlinear model, MWD effect is employed. The empirical parameters used in the MWD modeling are dependent on the vehicle size and geometry thus effects of their variation is analyzed to tune the parameters for the current vehicle.

In Figure 9, time constant used in the modeling of wake geometry dynamics is studied. Default value (τ_{RW}) is estimated using the empirical equation (1).

Alternative solutions are also estimated by perturbing this value 20% up and down to demonstrate the response sensitivity due to this parameter in Figure 9. It shows that, if the system is more agile than expected (lower time constant) available stabilization on the system is not enough to damp out the oscillations. Likewise opposite of this statement is also true if the dynamics are slower than expected due to higher time constant. It is notable that either one of these three cases can match the frequency observed in the test data, as well as the amplitudes match well, unless they are diverged or converged. Also the phase between the pitch and roll oscillations, which is approximately 90 degrees, found in the analyses matched well with the flight test data as shown in Figure 2. Therefore closed loop dynamics of the model is thought to be a well enough representation of the test vehicle.

Pitch and roll rates related parameters of the model are scaled by the ratio between the default and estimated time constant of the model at first, but needs to be further tuned to obtain matching data with the flight test. As a result of this tuning a reference value "k_{pq}" is found which is roughly around one half of the ratio between the time constants. It is tuned so that similar results with the test and the model can be obtained. In Figure 10, its effect is studied. In case where 20% higher value is used, low amplitude but higher frequency oscillations observed in the model which are not present in the flight test data. Though similar oscillations can be seen in the beginning of the test data starting at 310 second time stamp, they are rapidly damped out in less than 5 seconds. Using a 20% lesser value for the "k_{pq}" scale factor caused unstable solutions as shown in the same figure.

Briefly in this section empirical value for the time delay is used and the other empiric parameters are scaled till observing stable and consistent solutions. As a result of this study on the MWD parameters amplitude, frequency and phase between the pitch and roll oscillations are matched to the test data, as well as the same level of stability is achieved in the model that matched the hovering test data.

3. ANALYSES

3.1. Forward Flight Trim and Fly-Bar Control Load Alleviation

In this section trim analyses are carried out for hover and low speed forward flight. Trim analysis is a steady state solution found by iterating the control inputs to match the desired flight conditions, driving the translational and rotational accelerations to zero while body states are frozen in time. Therefore transients are omitted in these analyses, yet contribution of the fly-bar can still be observed. At this stage steady-state convergence parameters are adjusted, such as minimum number of rotor revolutions and the number to average.

Figure 3 shows the main rotor and tail rotor collective values during forward flight trim analysis. Typical parabolic trend for the main rotor collective variation due to increasing flight speed can be observed. Maximum endurance and maximum range flight speeds can be addressed from this figure, 20 m/s and 30 m/s, respectively. Tail rotor collective also shows a typical trend where it follows the main rotor collective till midway then it stays low due to fuselage/empennage aerodynamics apparent on the vehicle.

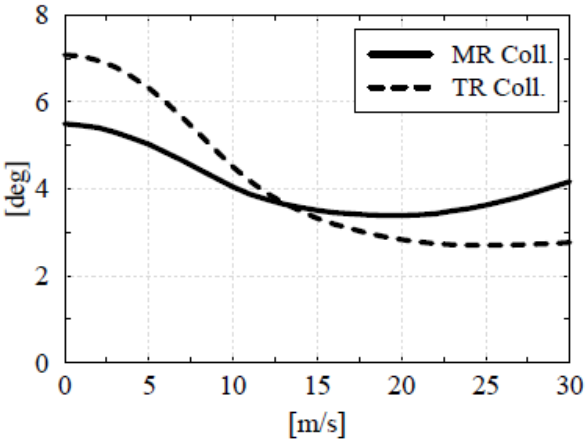

Figure 3 Main rotor and tail rotor collective variation in forward flight trim

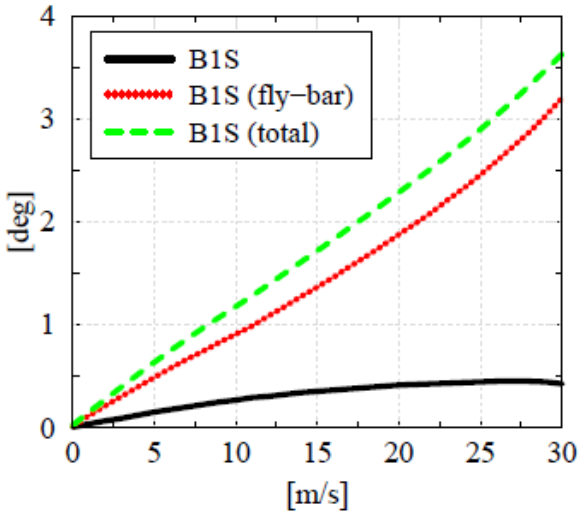

Figure 4 Longitudinal cyclic variation in forwad flight trim

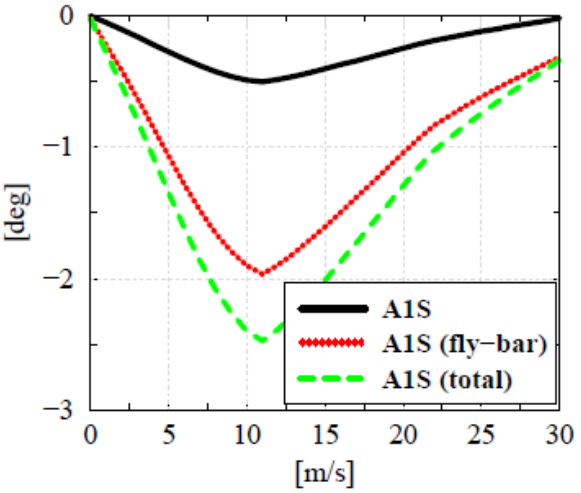

Figure 5 Lateral cyclic variation in forwad flight trim

Figure 4 and Figure 5 shows the longitudinal and lateral cyclic trim values, respectively. Longitudinal cyclic value shows a monotonic increase trend as expected but the values are significantly smaller than those typically found on a conventional system. This is associated with the fly-bar contribution therefore effective cyclic inputs (B1S-total) experienced by the main rotor are estimated by employing the harmonic analysis on the periodic pitching data, and consequently fly-bar contribution (B1S-fly-bar) shows up as the difference between the effective cyclic input and the given input (B1S) through the swashplate. It is also important to note that, cyclic inputs adopted by fly-bar have a maximum of 25 degrees whereas direct control of the main rotor blades is only 4 degrees at the same control level. Therefore there is always higher contribution of the fly-bar controls over the main rotor compared to the direct control.

As a result of this section fly-bar contribution to the cyclic inputs can be drawn for every flight speed separately. In terms of control load alleviation, maximum gain is achieved at higher speeds such as 20 m/s where it reaches up to 80%. It is also noted that the required longitudinal input starts to have a negative gradient at speeds roughly about 25 m/s which sets a limitation for the usage of fly-bar at high speeds.

3.2. Eigenvalue Analysis

Eigenvalue analysis of the system is performed for hover and low speed forward flight. Eight body states (pitch, roll, three body velocities and three rotational rates) are selected for the model order reduction. Linearization is performed over one rotor revolution for every azimuthal step then system matrices are averaged. This methodology is best suited for the hover and low speed cases since time periodicity is at its lowest levels. Developed nonlinear model is taken into account as the baseline in this section and two additional alternative models are created, same model without the fly-bar in effect and the other one with equivalent feedback of the fly-bar on this later model.

In Figure 11, eigenvalues are shown for hover with the reduced order linear models of the baseline and its two alternatives. Fly-bar system accounted for in the baseline inherits a stability which clearly showed up here when its eigenvalues compared to those of the "no fly-bar" case. Moreover, baseline model eigenvalues are very closely matched when the identified feedback gains used on the "no fly-bar" model system matrices, also confirming the identified gains as well as the classic methodology to model the fly-bar.

Figure 12, shows the eigenvalues of the reduced order linear system extracted from the baseline model for low speed (10 m/s) forward flight. It is important to notice that feedback gain used to represent fly-bar failed at capturing two conjugate eigenvalues at this condition. Though that mode can be omitted since it is a highly damped one it is important to note that only advanced modeling of the fly-bar can capture such differences.

3.3. Stall Conditions of the Fly-bar Blades During Forward Flight

Similar vehicles to the one used in this study tend to have maximum speeds corresponding to approximately 0.2 advance ratio (μ) which is lower than the usually experienced maximum advance ratio for conventional helicopters. Controls and

stability are dependent on the fly-bar dynamics therefore degradation of the aerodynamics around this smaller rotor located at the center of the main rotor is thought to be the source of this limitation. In order to explore the aerodynamic degradation, specifically stall condition, forward flight trim analyses are revisited in this section. Since each trim result at any specified flight speed is due to the periodic solution of the main rotor, fly-bar angle of attack fluctuates at the same frequency as well. Therefore, maximum and minimum values experienced on them are plotted in Figure 6. It is noted in this figure that stall conditions starts around 25 m/s (~0.16 advance ratio), considering low Reynolds number onset the stall angle of attack at lower values. Besides, it is seen in the same figure that rapid decrease in the minimum angle of attack experienced by the fly-bar blade starts at 12 m/s which should be considered as a scheduling break point for the controller design. It is also evident from the figure that providing some pitch offset (it can be regarded as collective) on the fly-bar blades should offset the stall speed though it would be limited around 5-10 m/s most. Even this would not bring the maximum advance ratio above 0.25.

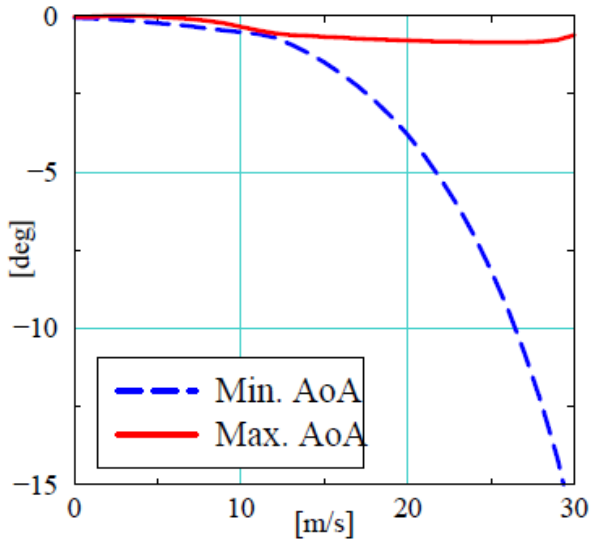

Figure 6 Maximum and minimum Angle of Attack on fly-bar blades for forward flight speeds

3.4. Time Response due to Disturbance

In this section an isolated rotor model of the fly-bar is used to explore the input/output relations of this system. Inputs are taken as swashplate cyclic controls over the fly-bar and the teetering angle is the output which adds up to the main rotor controls on the full rotorcraft. Figure 7 and Figure 8 shows the amplitude ratio and phase between the cyclic input and teetering output of the fly-bar system, respectively. Amplitude ratio of unity starts to deteriorate when cyclic inputs are over 5 degrees whereas phase drifts away from 90 degrees, both showing that the system is no longer linear. This condition too requires a breaking point in the scheduling of the controller since it would bring some coupling in the outputs as well as its efficiency would be compromised.

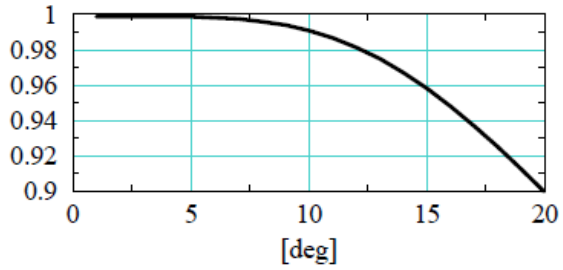

Figure 7 Amplitude ratio due to cyclic input

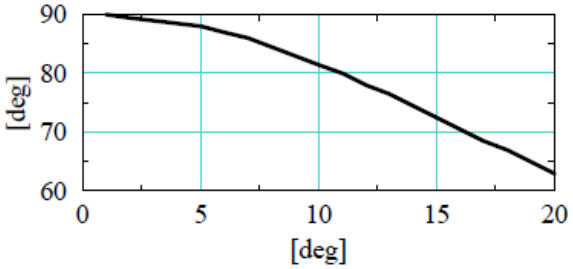

Figure 8 Phase response due to cyclic input

4. CONCLUSION

In this study a comprehensive model of a rotary-wing unmanned aerial vehicle is built. Though it is a small size vehicle with a more conservative flight envelope compared to conventional helicopters, there are still critical issues related with this system that needs comprehensive nonlinear modeling. Maneuver wake distortion and its effect on the vehicle dynamics, fly-bar system as a standalone rotor are major concerns to address by comprehensive modeling for this type of system. It is also shown that comprehensive modeling of this system brings up opportunities to improve typical drawbacks such as forward flight speed limitation and controller design with safer flight testing as well as reduction in the flight test times.

Some future work opportunities are also explained in the following paragraphs which are omitted in this study.

Stall condition of the fly-bar blades is identified through the forward flight trim analysis. Once these blades experience the stall conditions system controllability and stability would be altered significantly, therefore this is assumed as a solid limitation on the forward flight speed. It would be

possible to explore flying characteristics beyond this point if a dynamic stall model is employed on the fly-bar rotor blades. This might be used in a study exploring stall recovery options.

Main rotor controls and stability are provided mostly by the fly-bar through mechanical relation between its tilt and main rotor controls. In this regard, only the kinematics of the feathering degree of freedom of the main rotor blades considered in this study. Actually, there also exists a dynamic relation between the fly-bar tilt and pitching moment of the main rotor blades which can be included in the future studies similar to the modeling of control stiffness.

ACKNOWLEDGMENTS

Author would like to thank the flight testing and mechanical testing team members of the ASELSAN-MGEO for their successful work.

REFERENCES

[1] FLIGHTLAB Theory Manual (Vol. I-II), Advanced Rotorcraft Technology, Inc., July, 2011.

[2] Padfield,G. D., "Helicopter Flight Dynamics: The Theory and Application of Flying Qualities and Simulation Modeling," Blackwell Publishing, Oxford, United Kingdom, 2007.

[3] Prasad, J.V.R., Nowak, Margon, and Xin Hong, “Finite State Inflow Models for a Coaxial Rotor in Hover”, 38th European Rotorcraft Forum, Amsterdan, Netherlands, 2012

[4] Olcer, F.E., “Development of a Neural-Network (NNET) Based Engine Model”, AHS 70th Annual Forum, Montreal, Quebec, Canada, May 20-22, 2014.

[5] Kim, S.K., Tilbury, T.M., “Mathematical Modeling and Experimental Identification of an Unmanned Helicopter Robot with Flybar Dynamics”, Journal of Robotic Systems, 21(3), pp. 95-116, 2004.

[6] Zhao, J., Prasad, J.V.R., Peters, D.A., “Validation of a Rotor Dynamic Wake Distortion Model for Helicopter Maneuvering Flight Simulation”, Journal of the American Helicopter Society, Vol. 49, No. 4, pp. 414-424, October, 2004.

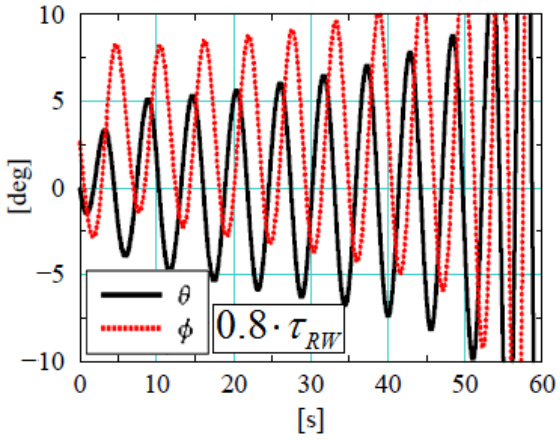

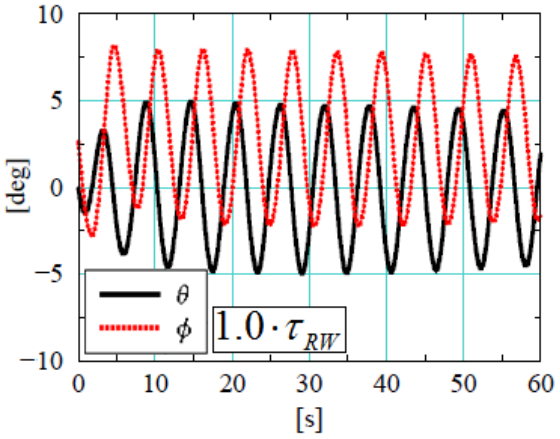

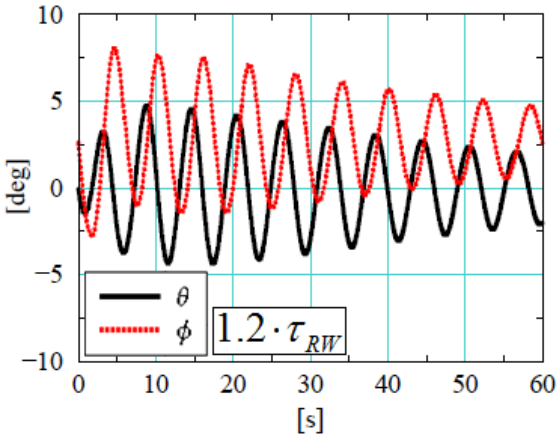

Figure 9 Effect of Time Delay due to Maneuver Wake Distortion

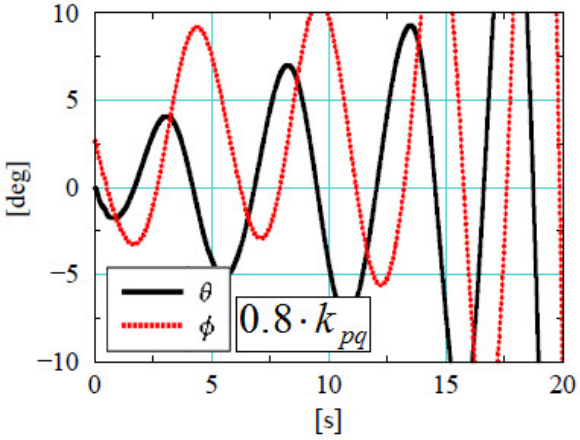

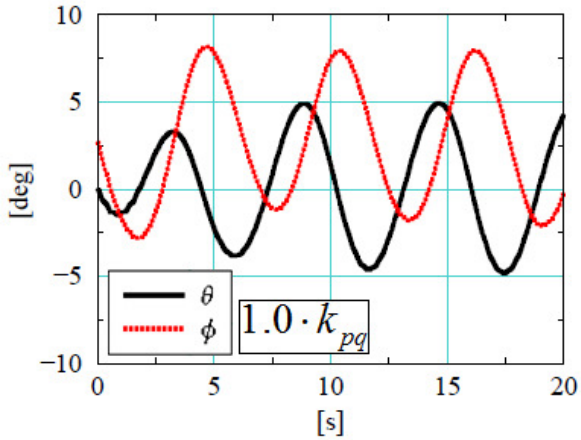

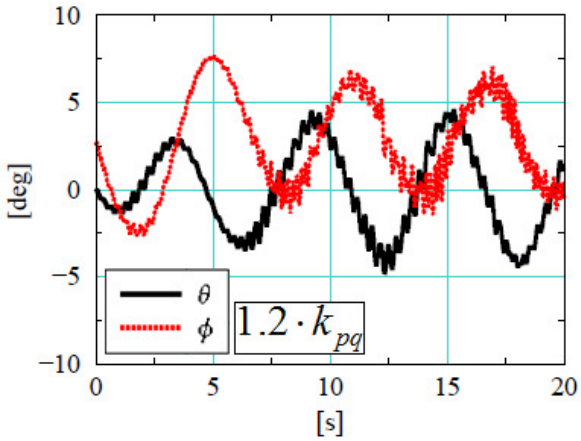

Figure 10 Effect of Rotational Rate Parameters due to Maneuver Wake Distortion

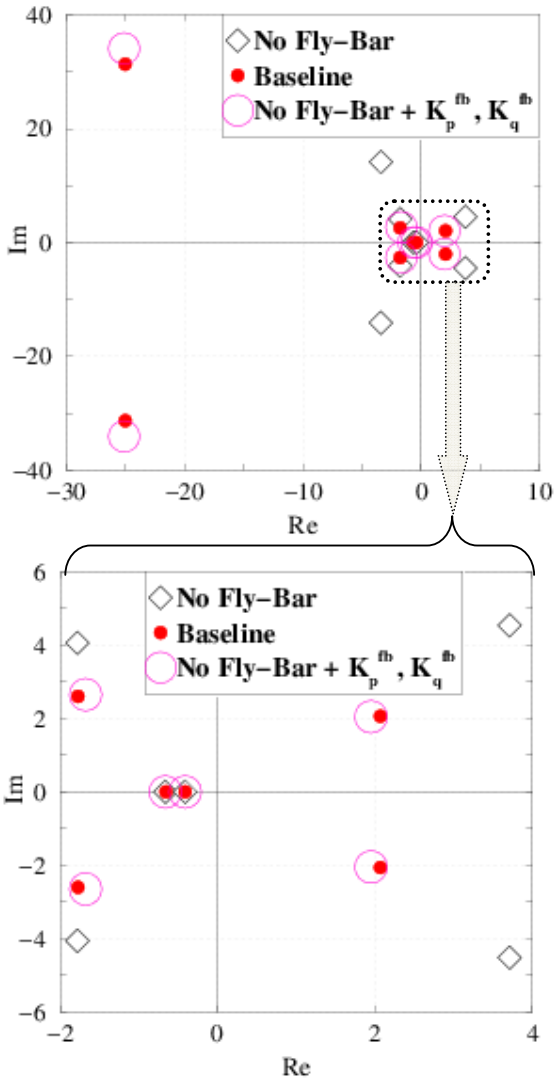

Figure 11 Eigenvalues at hover

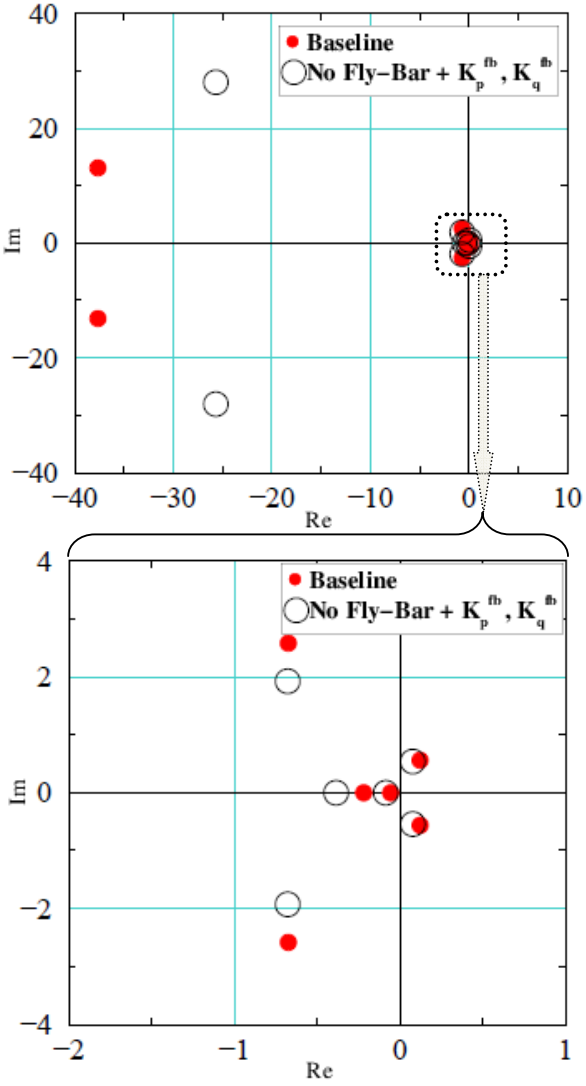

Figure 12 Eigenvalues at low speed flight